THE JOURNAL OF PHYSICAL CHEMISTRY C

Article

pubs.acs.org/JPCC

Facile Microwave-Assisted Synthesis of Multiphase $CuInSe_2$ Nanoparticles and Role of Secondary CuSe Phase on Photovoltaic Device Performance

Yeong-Hui Seo,[†] Byung-Seok Lee,[‡] Yejin Jo,[†] Han-Gyeol Kim,[†] Youngmin Choi,[†] SeJin Ahn,[§] KyungHoon Yoon,[§] Kyoohee Woo,[∥] Jooho Moon,[∥] Beyong-Hwan Ryu,[†] and Sunho Jeong*,[†]

[†]Advanced Materials Division, Korea Research Institute of Chemical Technology (KRICT), 141 Gajeongro, Yuseong, Daejeon 305-600, Korea

[‡]Advanced Materials Lab, Global Technology, SK Innovation, 325, Exporo, Yuseong, Daejeon 325-712, Korea

[§]Solar Energy Department, Korea Institute of Energy Research (KIER), 71-2 Jang-dong, Yuseong-gu, Daejeon 305-343, Korea

[∥]Department of Materials Science and Engineering, Yonsei University, 50 Yonsei-ro, Seodaemun-gu, Seoul 120-749, Korea

Supporting Information

ABSTRACT: Multiphase $CuInSe_2$ (CISe) nanoparticles including the secondary CuSe phase are synthesized by a polyol-based, microwave-assisted solvothermal method. It is demonstrated that the reaction chemistry involving formation of the CISe phase is adjusted depending on the heretofore unrecognized chemical nature of polyol solvent, allowing for formation of secondary CuSe phase-incorporated multiphase CISe nanoparticles. The critical role of CuSe phase in generating the pore-free, dense CISe absorber layer for a high-performance thin-film photovoltaic device is investigated through the comparative study on CISe absorber layers derived from both multiphase and single-phase CISe nanoparticles.

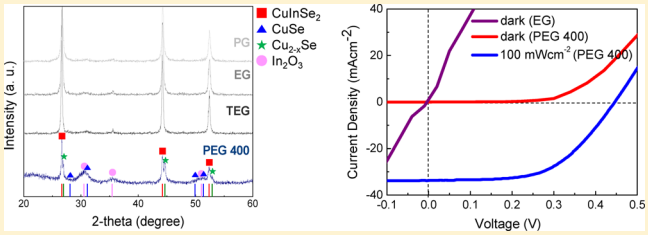

1. INTRODUCTION

Chalcopyrite compounds are considered promising materials for thin-film solar cells owing to their advantageous optical band gap and high absorption coefficient for solar radiation.[1,2] In general, high-performance absorber layers have been fabricated by vacuum-based deposition methods such as multistage coevaporation and the two-step process of sputtering and selenization.[3] However, their high manufacturing costs are inhibitory to mass-produced, large-area solar cell applications. In contrast, solution-processed deposition methods can provide many advantages, such as a less-energy-intensive route, scalability, simplicity, and high throughput, enabling realization of high-performance, low-cost solar cell applications.[4]

Recently, the solution-processed $Cu(In,Ga)Se_2$ (CI(G)Se) solar cell with a high conversion efficiency of ~15.2% was reported based on utilization of hydrazine as a solvent for dissolving the specific, impurity-free precursors.[5] However, hydrazine-based approaches are toxic and explosive; thus, they should be handled with adequate protective measures.[6] As an alternative, chemical methods based on CI(G)Se nanoparticles have been extensively explored for creation of solution-processed absorber layers.[1,7,8] However, in spite of numerous in-depth investigations on the chemical and physical nature of CI(G)Se nanoparticles, poor device performance has been reported due to inefficient charge carrier transportation in porous nanocrystal films.[7] In addition to elemental stoichiometry, surface morphology, and high crystallinity, formation of pore-free dense absorber layer is a prerequisite for significantly improving device performance.[9] Recently, it has been demonstrated that nanoparticle-based, dense absorber layers could provide a thin-film photovoltaic device with a high conversion efficiency of ~12% through a unique chemical approach based on pore filling in particulate layers by replacing S with Se.[10]

Another effective pathway for generating high-performance, dense absorber layers is thermal triggering of grain growth by a low-melting-point CuSe phase. For vacuum-deposited absorber layers, CuSe is a well-known low-melting-point phase (T_m of the CuSe phase is 523 °C) for creating a high-performance CI(G)Se absorber. However, to date, use of the CuSe phase in colloidal-processed CI(G)Se absorber layers has rarely been demonstrated due to difficulties in synthesizing metastable CuSe nanoparticles. Furthermore, even with successful synthesis of CuSe nanoparticles, formation of a stoichiometry-controlled CI(G)Se absorber layer remains challenging. Precisely controlled incorporation of In-rich selenides is required to adjust the stoichiometry of the CI(G)Se layer. Recently, it was demonstrated that the CuSe phase is

Received: October 22, 2012
Revised: April 9, 2013
Published: April 9, 2013

 © 2013 American Chemical Society

synthesized on the surface of InSe nanoparticles, resulting in InSe−CuSe core−shell nanoparticles.[11] However, the poor device performance with conversion efficiency of 1.1% was demonstrated owing to the poor microstructure of the CISe absorber layer. In addition, this method has another drawback that the stoichiometry of the CISe layer should be tailored by controlling the relative volume fraction of the InSe core and CuSe shell layer.

In synthesizing the metastable phase nanoparticles, kinetic control of chemical reactions is inevitably required. The microwave synthetic method would allow for kinetic control of reaction chemistries through the instant, controllable supply of thermal energy. For general solvothermal methods, commonly used for synthesis of functional nanoparticles, the heating rate is hard to control accurately, especially in the case of extremely rapid heating, even with a hot-injection technique. In addition, the microwave synthetic method provides various advantages, such as a short reaction time, excellent reproducibility, and high yields of products.[12] However, most research on microwave-based synthesis of chalcopyrite materials has been mainly directed toward formation of morphology-controlled, phase-stable, stoichiometric nanoparticles, including binary chalcogenide nanoparticles.[13] To date, except for our recent report,[14] working devices have not been demonstrated using CI(G)Se nanoparticles synthesized by microwave synthesis due to the lack of a synthetic strategy for incorporating the low-melting point, metastable CuSe phase in the CI(G)Se nanoparticle system.

In this study, we report the microwave irradiation-based chemical methodology for synthesizing metastable CuSe phase-including multiphase CISe nanoparticles that facilitate fabrication of a solution-processed, high-performance absorber layer. It is demonstrated that the crystalline-phase evolution during microwave-induced synthesis is predominantly determined by the chemical nature of the polyol solvent, enabling reproducible synthesis of metastable CuSe phase-including multiphase CISe nanoparticles. The critical role of the CuSe phase on generation of device-quality absorber layers is clarified by comparing the device performance of a CISe thin-film photovoltaic device derived from either CuSe phase-free or CuSe phase-including CISe nanoparticles.

2. EXPERIMENTAL SECTION

2.1. Raw Materials. All reagents for metal source, copper(II) acetate monohydrate ($Cu(CO_2CH_3)_2{\cdot}H_2O$, 98+ %,), indium(III) acetate ($In(C_2H_3O_2)_3$, 99.99%), and selenium powder (Se, 99.99%) were purchased from Aldrich and used as received without further purification. Propylene glycol (PG, Aldrich, $CH_3CH(OH)CH_2OH$, ≥99.5%), ethylene glycol (EG, Aldrich, $HOCH_2CH_2OH$, 98%), triethylene glycol (TEG, Aldrich, $HO(CH_2CH_2O)_2CH_2CH_2OH$, 99%), and polyethylene glycol 400 (PEG 400, Junsei, $H[OCH_2CH_2]_nOH$, M_w = 400, extra pure) were used as solvents. Polyvinylpyrrolidone (PVP, Aldrich, $(C_6H_9NO)_n$, M_w = 55 000) was incorporated as an organic additive in preparing the CISe nanoparticle ink.

2.2. Microwave-Assisted Synthesis of Multiphase CISe Nanoparticles. A 0.6 g (2.9 mmol) amount of copper(II) acetate monohydrate, 1.43 g (4.9 mmol) of indium(III) acetate, and 0.75 g (9.8 mmol) of selenium powder were dissolved in 20 g of PEG 400. After stirring for 1 h at room temperature, the precursor solution was transferred to the Teflon liner vessel and heated under MW irradiation. Upon completion of the synthesis reaction, the reaction solution was cooled to room temperature and nanoparticles were separated by centrifugation, collected, and washed three times with ethyl alcohol. Then, the resulting nanoparticles were dried under vacuum overnight at 40 °C to provide black powders.

2.3. Microwave-Assisted Synthesis of Single-Phase CISe Nanoparticles. A 0.8 g (4.0 mmol) amount of copper(II) acetate monohydrate, 1.43 g (4.9 mmol) of indium(III) acetate, and 0.75 g (9.8 mmol) of selenium powder were dissolved in 20 g of polyol solvent (PG, EG, or TEG). After stirring for 1 h at room temperature, the precursor solution was transferred to the Teflon liner vessel and heated under MW irradiation. Upon completion of the synthesis reaction, the reaction solution was cooled to room temperature and nanoparticles were separated by centrifugation, collected, and washed three times with ethyl alcohol. Then, the resulting nanoparticles were dried under vacuum overnight at 40 °C to provide black powders.

2.4. Ink Preparation and Solution-Processed Film Deposition. For preparing the ink, nanoparticles with a solid content of 20 wt % were added in a mixed solvent with 0.76 g of ethyl alcohol and 1.68 g of EG, and PVP was added as an organic additive to form a crack-free layer. The prepared ink was mixed by ball milling to break softly agglomerated nanoparticles and then deposited on Mo-coated soda lime glass substrate. The resulting thin film was dried at 80 °C in a vacuum oven. For thermal decomposition of PVP and microstructural/compositional evolution of films, selenization was carried out in a vacuum evaporator equipped with a Knudsen-type effusion cell. The chamber was evacuated to a base pressure of 5×10^{-6} Torr, and elemental Se was evaporated. The flux of Se vapor was adjusted by the effusion cell temperature, and Se was effused at 180 °C. Samples were selenized at 530 °C for 30 min on a hot plate located in a chamber.

2.5. Solar Cell Fabrication. The CISe absorber layer selenized at 530 °C was integrated into a photovoltaic device following standard procedures, including chemical bath deposition of CdS (60 nm), RF sputtering of i-ZnO (50 nm), RF sputtering of Al-doped n-ZnO (500 nm), and thermal evaporation of the patterned Al grid as a current collector. The antireflection layer was not deposited for the devices tested in this study. Finally, devices were mechanically scribed into individual cells with a total active area of 0.44 cm^2. The conversion efficiency of the device was characterized using a class AAA solar simulator (WXS-155S-L2, WACOM, Japan).

2.6. Characterization. Morphological property, crystalline phase, and composition of multiphase CISe nanoparticles were analyzed using field emission scanning electron microscopy (FE-SEM, JSM-6700F, JEOL), X-ray diffraction (XRD, D/Max 2200 V/PC, Rigaku), and inductively coupled plasma mass spectrometry (ICPMS, Thermo Scientific iCAP 6500), respectively. The TEM image and TEM-EDS compositional profile for CuSe phase-including multiphase CISe nanoparticles were analyzed using a field emission transmission electron microscope (FE-TEM, Tecnai F20, Philips). The chemical interaction of polyol solvents with metal cations is proven from the FT-IR (Bruker vertex 80 V FT-IR Spectrometer, Bruker) and TGA result for as-prepared nanoparticles. The composition and phase transformation of CISe films after selenization were analyzed by energy-dispersive X-ray spectroscopy (EDS, Quantax 200, Bruker) and XRD measurement, respectively. The composition profile in CISe layer selenized at 530 °C

dx.doi.org/10.1021/jp310434j | J. Phys. Chem. C 2013, 117, 9529−9536

under Se atmosphere was characterized using scanning ion mass spectrometry (SIMS, IMS 7f, CAMECA).

3. RESULTS AND DISCUSSION

3.1. Synthesis of Multiphase $CuInSe_2$ Nanoparticles Including Secondary CuSe Phase. Hydroxyl groups are suitable for ionic conduction during microwave reactions[15] because of their high dipole moment; thus, the presence of an alcoholic- or polyol-based medium improves the performance of the microwave-based synthetic method, effectively converting the electromagnetic energy into heat.[16] However, since the reaction temperature at which the chalcogenide compounds are formed from precursor molecules is even higher than the boiling points of alcohols, the polyol solvents were used as a reaction medium for microwave-based crystal growth. In order to investigate the chemical role of polyol solvents on the crystalline phase evolution of CISe-based nanoparticles, propylene glycol (PG), ethylene glycol (EG), triethylene glycol (TEG), and polyethylene glycol 400 (PEG 400) were used as a solvent for dissolving the precursors and as a medium for absorbing microwaves. The chemical formula and properties of polyol solvents are summarized in Table 1. All polyol solvents

Table 1. Chemical Formula and Properties for Polyol Solvents Tested in This Study

solvent	chemical formula	boiling point (°C)	density (g/cm^3)	no. of hydroxyl groups per unit gram (#/g)
EG	$HOCH_2CH_2OH$	197	1.113	0.032
PG	$CH_3CH(OH)CH_2OH$	188	1.036	0.026
TEG	$HO(CH_2CH_2O)_2CH_2CH_2OH$	285	1.1	0.013
PEG 400	$H[OCH_2CH_2]_nOH$, $n = 9$	>250	1.128	0.005

have 2 hydroxyl groups in common at both ends. The distinct chemical difference among the solvents is the molecular weight along with the number of carbons between both of the chain-ending hydroxyl groups. The number of hydroxyl groups per unit gram is 0.032, 0.026, 0.013, and 0.005 for EG, PG, TEG, and PEG 400, respectively. A higher content of hydroxyl group improves the capacity for microwave-based effective heating by enabling the rapid heating of reaction mediums. For synthesizing the CuSe phase-including multiphase CI(G)Se nanoparticles, both reaction kinetics should be controlled: transformation of preformed Cu−Se and In(Ga)−Se compounds into the CI(G)Se compound and phase evolution of metastable CuSe into stable Cu_2Se phase. Both kinetics are fast at the elevated temperature at which the chalcogenide compounds are chemically formed from precursors, so that rapid heating is of critical importance for preserving the metastable phases. However, as shown in Figure 1, even the synthetic method based on EG, which has the highest amount of hydroxyl group, led to an almost completely transformed CISe pure crystalline phase. The major diffraction peaks of the chalcopyrite CISe phase, which can be indexed to (112), (220), and (312), match well for the nanoparticles synthesized in this study. CuSe and In_2O_3 phases appeared to be present when the PG, EG, or TEG was used as a solvent medium. However, their intensities in XRD patterns were negligible, and these phases, existing only in extremely small amounts, do not play a determining role in creating a device-quality, dense absorber layer, which will be

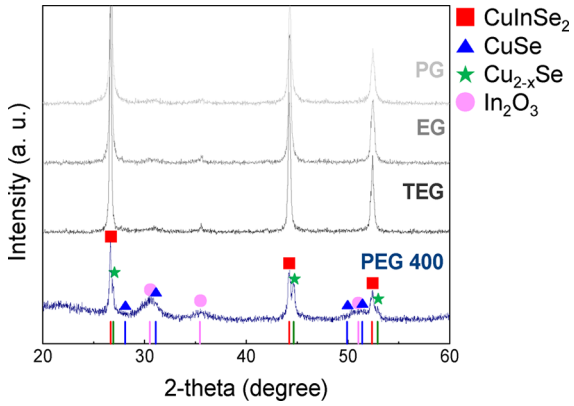

Figure 1. XRD patterns for CISe nanoparticles synthesized using different polyol solvents: PG, EG, TEG, and PEG 400.

proven with analysis of device performance. This implies that, by itself, the heating rate control is not sufficient to preserve the metastable or intermediate phases prior to complete transformation into stable phases. In contrast, in the case where PEG 400 was used, multiphase CISe nanoparticles, which consists of CuSe, $Cu_{2-x}Se$, and In_2O_3 as secondary phases, were synthesized. The resulting CuSe phase-including multiphase CISe nanoparticles were spherical in shape, as shown in Figure S1, Supporting Information. The average particle size was measured to be 80 nm. Formation of multiphase CISe nanoparticles was also confirmed by TEM-EDS compositional profile analysis (Figure S2, Supporting Information). It was tentatively revealed that the 80 nm sized nanoparticle is composed of fine aggregates of various phases including the CuSe phase. Rapid phase transformation can be suppressed by preventing mass transport between preformed intermediate compounds. The polyols interact with the metal cations by forming chemical bonding between the metal cation and the deprotonated polyol molecule,[17] attaining surface capping by polyol molecules on resulting nanoparticles. Chemical interaction of polyol solvents with metal cations was proven from the FT-IR and TGA result for as-prepared nanoparticles. In FT-IR spectra for as-synthesized nanoparticles (Figure 2), the presence of polyol molecules (EG and PEG 400) as a capping molecule was confirmed by the bands due to C−C deformation vibration at 880 cm^{-1}, C−O stretching at 1200−1000 cm^{-1}, O−H stretching at 3412 cm^{-1}, and C−H stretching in the range of 3000−2800 and 1500−1400 cm^{-1}.[18] The wide bands in the range of 3700−3000 and 1600 cm^{-1} are attributed to bending vibrations of water adsorbed from moisture in the air during pellet preparation. In TGA result (Figure 3), weight loss proceeded up to 300−400 °C under inert atmosphere, indicative of the presence of chemical moieties other than water molecules. Owing to the absence of additional capping molecules, the chemical moieties that can be adsorbed on the resulting nanoparticles are only the polyol molecule and the adsorbed water molecule that is evaporated below 200 °C. Thus, it is speculated that the Cu, In cations are functionalized chemically by polyol molecules, and the chemical nature of Cu, In cations is determined by the chemical structure of the polyol molecules. As the number of carbons in polyol molecules increases, the chain length bonded chemically with metal cations becomes longer, which leads to a stronger steric hindrance against the chemical reaction capability of Cu, In metal cations. As the chain length of polyol molecules is long enough to endow the steric hindrance, the mass transport

dx.doi.org/10.1021/jp310434j | J. Phys. Chem. C 2013, 117, 9529−9536

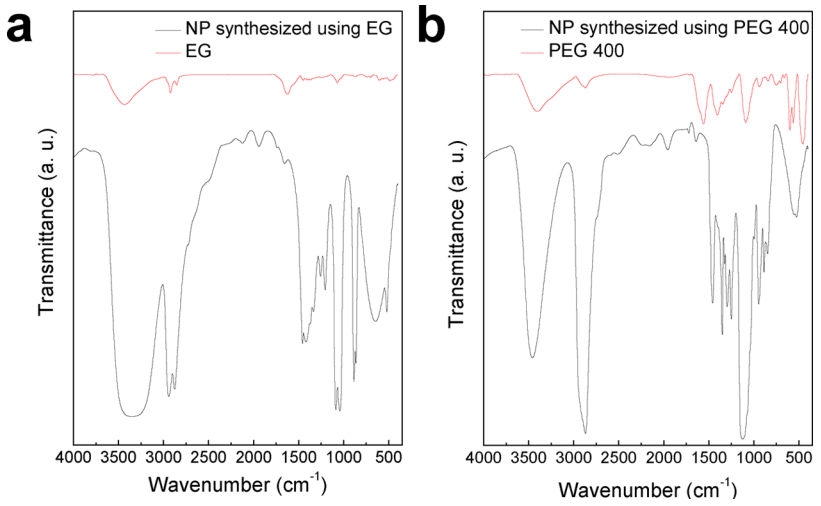

Figure 2. FT-IR spectra for (a) EG and nanoparticles synthesized using EG and (b) PEG 400 and nanoparticles synthesized using PEG 400.

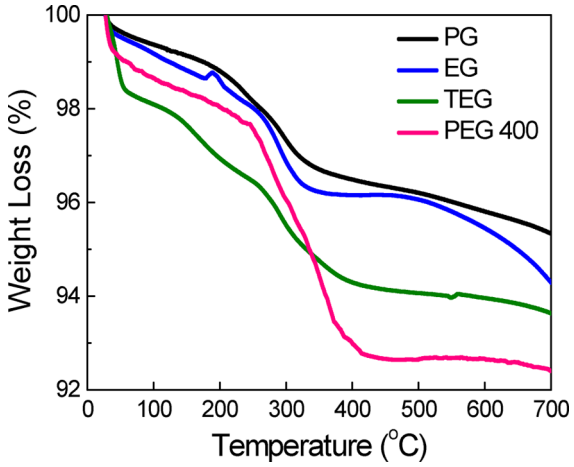

Figure 3. Thermal gravimetric analysis curves (under N_2 atmosphere) for as-synthesized CISe nanoparticles.

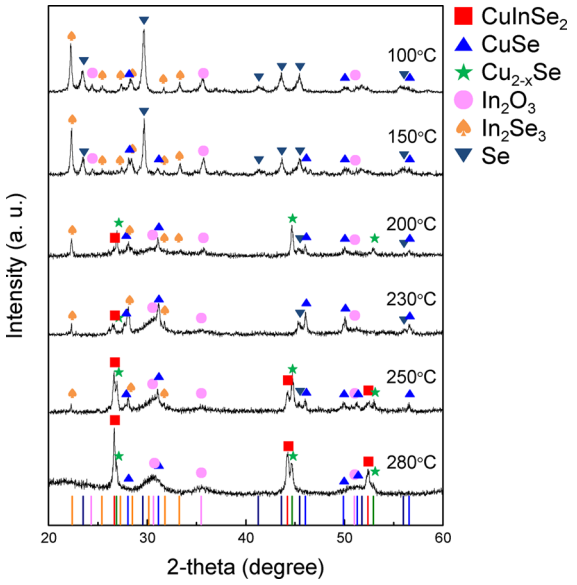

Figure 4. XRD patterns for CISe nanoparticles synthesized using PEG 400 at various temperatures: 100, 150, 200, 230, 250, and 280 °C.

between preformed compounds becomes suppressed, which gives rise to a kinetic controllability on the presence of the metastable crystalline phase. As shown in Figures 4 and 5, when PEG 400 was used as a solvent medium, transformation of the intermediate phases into stable phases was easily tailored, depending on reaction time and reaction temperature. When the reaction time was maintained at 25 min, the intermediate phases were mainly present below 230 °C and the CISe phase started being formed above 250 °C, consuming the secondary phases (Figure 4). In the case of an instant reaction at 280 °C, the CISe phase was slightly formed and transformation into the CISe phase proceeded further when the reaction was maintained for 25 min at 280 °C (Figure 5). In terms of the presence of both the main CISe phase and the secondary CuSe phase, the synthesis condition, with a reaction temperature of 280 °C and reaction time of 25 min, made it possible to form the multiphase nanoparticle system suitable for creation of a device-quality CISe absorber layer. In contrast, for other polyol-based synthetic methodology, crystalline phase evolution was hardly controlled. Only a complete CISe phase was predominantly observed, regardless of the reaction time above temperatures at which the chalcogenide compounds are formed. According to the result of inductively coupled plasma mass spectrometry analysis, the composition of the multiphase CISe nanoparticles was measured to be Cu:In:Se = 29:43:28 and the molar ratio of Cu to In was 0.67. In a reaction batch, the ratio of Cu acetate to In acetate was 0.6. Yields for elemental In and Se in CuSe phase-including multiphase CISe nanoparticles were 89 and 29%, respectively. The slight deficiency of In is attributed to loss of unreacted In precursor, and the deficiency of Se is associated with the presence of secondary phases including In_2O_3. The composition of single-phase CISe nanoparticles, synthesized using PG, EG, and TEG, was Cu:In:Se = 0.8:1:2.

3.2. Role of Secondary CuSe Phase in Developing the Device-Quality Absorber Layer. For an in-depth investigation on how the presence of the CuSe phase in a colloidal-processed particulate layer predominantly influences the microstructural characteristics of absorber film and device performance, two distinctively different inks were formulated using nanoparticles synthesized using either EG or PEG 400. For preparing the inks, nanoparticles were dispersed in a mixture of ethylene glycol and ethanol. The CISe layers were coated on cleaned Mo-coated soda lime glass substrate. The

dx.doi.org/10.1021/jp310434j | J. Phys. Chem. C 2013, 117, 9529−9536

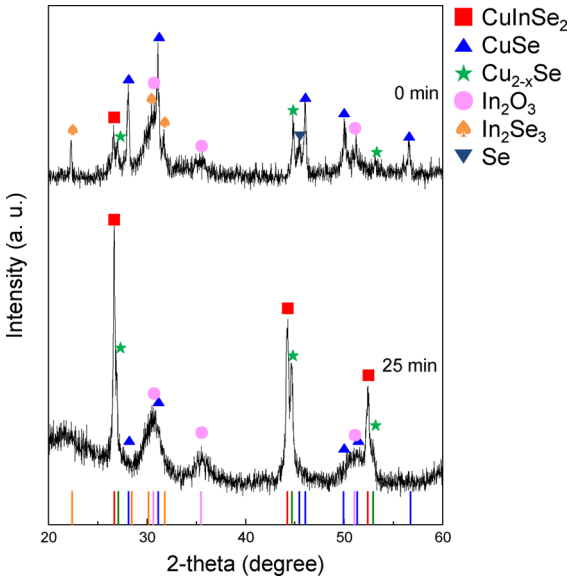

Figure 5. XRD patterns for CISe nanoparticles synthesized using PEG 400 at 280 °C for 0 and 25 min (atomic ratio), which correspond well with the composition of precursors.

CISe phase is thermally decomposed at an elevated temperature in air due to loss of Se in the form of volatile SeO_2; thus, the coated CISe layers were annealed under Se atmosphere to suppress loss of Se. For the absorber layer prepared from single-phase CISe nanoparticles (synthesized using EG), formation of volatile species and phase transformation during selenization at 530 °C did not occur. In contrast, for the absorber layer prepared from multiphase CISe nanoparticles (synthesized using PEG 400), the chemical structural and compositional evolution was evolved during selenization at 530 °C, accomplishing production of a device-quality CISe absorber layer suitable for a highly efficient thin-film solar cell. In_2O_3 was converted to In_2Se_3 and in turn involved in phase transformation into $CuInSe_2$ by the thermally enhanced reaction with copper selenide compounds, which led to the highly crystallized, single-phase (secondary-phase free) CISe layer (Figure 6). The ratio of Cu to In was also adjusted to 0.8 by the subtle loss of In in the form of In_2Se (g), commonly observed even in vacuum-deposited films,[19] affording the optimum composition (Cu:In:Se = 0.8:1:2) for a high-performance CISe

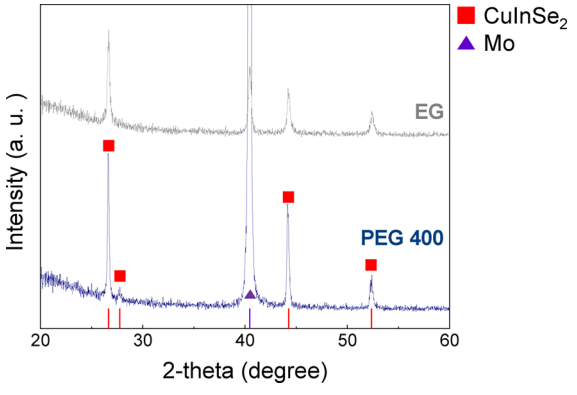

Figure 6. XRD patterns for the solution-processed CISe absorber layer (selenized at 530 °C) prepared with the single-phase CISe nanoparticles (synthesized using EG) and multiphase CISe nanoparticles (synthesized using PEG 400).

absorber layer. This compositional change during selenization was reproducible, and the composition deviation among the CISe absorber layers selenized at 530 °C was negligible. Compositional deviations for 8 identical samples were studied, and it was proven that the deviation was not out of an error range in EDS analysis. These results indicate that even though it is based on multiphase nanoparticles, the single-phase, composition-controlled absorber layer can be obtained, as derived from single-phase, stoichiometric CISe nanoparticles.

However, both selenized absorber films exhibited noticeably different microstructural properties. Figure 7 shows the

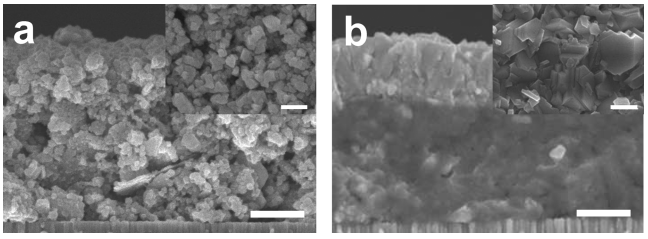

Figure 7. Cross-sectional SEM images for solution-processed CISe absorber layers (selenized at 530 °C) prepared using (a) single-phase and (b) multiphase CISe nanoparticles. (Insets) Top-view SEM images, and all scale bars are 500 nm.

representative cross-sectional SEM images of the absorber layer prepared from single- and multiphase CISe nanoparticles. As shown in Figure 7a, even after being annealed above 530 °C under Se atmosphere, the absorber film prepared from single-phase CISe nanoparticles was still composed of a porous particulate structure with a soft agglomeration between neighboring nanoparticles. Formation of a dense microstructure by grain growth did not take place. In contrast, for the absorber layer prepared from multiphase CISe nanoparticles, the void-free, fully dense absorber layer with large grains was evolved simply after selenization at 530 °C (Figure 7b). Once a liquid phase forms via melting of CuSe, a capillary pressure gradient, enough to induce rapid liquid flow and particle rearrangement, is generated. Consequently, the solid dissolves at the solid–liquid interfaces with a higher chemical potential, diffuses through the liquid, and precipitates on the particles at other sites with a lower chemical potential,[20] which allows for effective densification and crystallization. For high liquid high content, complete densification can be achieved by rearrangement alone, whereas at the low liquid contents common for many systems, the solid skeleton inhibits densification and the solution–precipitation step is required to achieve further densification. Densification by the solution–precipitation mechanism is accompanied by changes in the shape of the grains. For a small amount of liquid, the grain develops flat faces and the shape of polyhedron is generated for achieving more efficient packing. Thus, grains with various dihedral angles are detectable in a low-volume fraction of liquid, whereas the rounded grains are commonly observable in a moderate amount of liquid. As shown in a top-view SEM image for the selenized multiphase CISe film, grains showed a polyhedral morphological property, which implies that the solution–precipitation mechanism is dominant in the densification reaction. The melting points of secondary phases other than the CuSe phase are much higher than the processing temperature for the chalcopyrite-based thin-film solar cell (the melting points of In_2O_3 and Cu_2Se are 1910 and 1113 °C,

dx.doi.org/10.1021/jp310434j | J. Phys. Chem. C 2013, 117, 9529–9536

respectively); thus, the dramatic microstructural evolution into a completely dense absorber layer is attributable only to the CuSe phase, not to the other secondary phases. In Figure 7b, it was observed that the CISe layer is composed of a bilayer structure: the dense, well-crystallized layer with a thickness of 600 nm as an upper layer, and the amorphous-like layer as a lower layer with a thickness of 1 μm. Formation of a distinct bilayer structured film was confirmed by investigation of the elemental profile via secondary ion mass spectrometry (SIMS) analysis (Figure S3, Supporting Information). The lower layer contained the carbon-based impurities, unlike the carbon-free upper layer. It was also revealed that the composition is uniform vertically in a layered structure, indicative of no compositional and crystalline structural segregation in a CISe absorber film. As the dense CISe layer forms from the surface of the multiphase particulate layer, organic moieties, which result from complete thermal decomposition of the organic additive, are not evaporated through the preformed dense CISe layer and remain with the completely transformed CISe component. For solution-processed, crack-free chalcopyrite absorber layers this bilayer structure including the impurity layer is commonly generated, exhibiting the relatively high performance.[21] This formation of bilayer structure by incomplete evaporation of organic moieties is confirmed by the fact that the absorber layer, prepared from single-phase CISe nanoparticles, is free of the organic residual layer, which results from free evaporation of organic moieties through the porous microstructure. However, even with the presence of a residual layer, carriers transport through the chalcopyrite phase that was percolated in impurities and the electrons and holes are separated effectively at the junction between the CdS layer and the well-formed, impurity-free chalcopyrite layer. Optimization of the organic additive burning behavior is currently underway to form an organic residue-free absorber layer.

3.3. Determining the Effect of Multiphase CISe Nanoparticles on Device Performance. For clarifying the role of the CuSe phase in the nanoparticle system on device performance, the absorber layers prepared using either single-phase or multiphase CISe nanoparticles were integrated into a photovoltaic device (glass/Mo/CISe/CdS/i-ZnO/n-ZnO/Al). An antireflection layer was not deposited for the devices tested in this study. As shown in Figure 8, for the device employing the absorber layer prepared from single-phase CISe nanoparticles, undesirable dark $I-V$ characteristics with a large leakage current were observed, indicative of generation of a CdS−CISe junction unacceptable for photovoltaic devices. Both CdS and ZnO layers reached the Mo bottom-electrode layer through the uniformly distributed voids in the porous CISe layer, which results in an electrically conductive path in the device architecture.[14] In the case of the device with the absorber layer derived from multiphase CISe nanoparticles, neither the buffer nor the window layer are capable of penetrating the CISe layer, owing to the fully dense grain structure, which allows for acceptable p−n junction characteristic. Whereas the device employing the absorber layer prepared from single-phase CISe nanoparticles did not show photovoltaic performance, the device based on an absorber layer prepared from multiphase CISe nanoparticles exhibited a conversion efficiency measured to be 8.2% with an open-circuit voltage (V_{OC}), short-circuit current density (J_{SC}), and fill factor (FF) of 0.44 V, 33.7 mA cm^{-2}, and 55%, respectively. It is presumed that multiphase CISe nanoparticles facilitated the device-quality absorber layer for a high-performance thin-film photovoltaic device through composition adjustment, formation of secondary phase-free CISe crystalline phase, dramatic microstructural evolution into a pore-free absorber film with large grains, and establishment of a favorable p−n junction. This distinctly different performance for both devices establishes the fact that the presence of the low-melting-point CuSe phase is of practical importance in generating the solution-processed, device-quality absorber layer, as observed in vacuum-deposited chalcopyrite thin-film solar cells. It is expected that other chemical strategies for incorporating the metastable CuSe phase in chalcopyrite-based nanoparticle systems would further facilitate improvement of device performance.

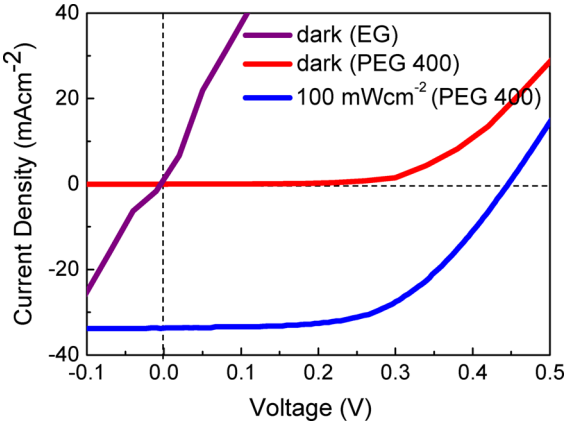

Figure 8. Light and dark $I-V$ device characteristics for a device employing the CISe absorber layer prepared from either single-phase or multiphase CISe nanoparticles. Light-illuminated $J-V$ characteristic was measured using a class AAA solar simulator (AM 1.5G, 100 mW cm^{-2}) at 25 °C.

4. CONCLUSION

CuSe phase-incorporated, multiphase CISe nanoparticles were synthesized by a microwave-assisted synthetic method. It was demonstrated that evolution of crystalline phases is determined by the chemical nature of polyol molecules that interact chemically with metal cations, in addition to polyol's chemical role as both a solvent for dissolving the precursors and a reaction medium for absorbing microwave energy. When PEG 400 was used as a polyol molecule, the kinetics on the transformation reaction of the intermediate phases into the CISe phase was adjusted easily, which allows for coexistence of a main CISe phase and secondary CuSe phase. From comparative analysis between the absorber layers derived from the CuSe phase-free CISe nanoparticles and the CuSe phase-included multiphase CISe nanoparticles, the critical role of the secondary CuSe phase in generating the device-quality chalcopyrite absorber layer was clarified.

■ ASSOCIATED CONTENT

Supporting Information

SEM images for CISe nanoparticles synthesized using either EG or PEG 400, HRTEM/EDS analysis for multiphase CISe nanoparticle, and SEM/SIMS analysis for CISe absorber layer derived from multiphase CISe nanoaprticles. This material is available free of charge via the Internet at http://pubs.acs.org.

dx.doi.org/10.1021/jp310434j | J. Phys. Chem. C 2013, 117, 9529−9536

AUTHOR INFORMATION

Corresponding Author

*E-mail: sjeong@krict.re.kr.

Notes

The authors declare no competing financial interest.

ACKNOWLEDGMENTS

This study was supported by a grant from the cooperative R&D program funded by the Korea Research Council Industrial Science and Technology and partially supported by the Industrial Core Technology Development Program funded by the Ministry of Knowledge Economy (No. 10031709, Development of Direct Nanopatterning Technology for Electronic Devices). This work was also supported by the National Research Foundation of Korea (NRF) grant funded by the Korea government (MEST) (No. 2012R1A3A2026417).

REFERENCES

(1) Yang, Y.-H.; Chen, Y.-T. Solvothermal Preparation and Spectroscopic Characterization of Copper Indium Diselenide Nanorods. *J. Phys. Chem. B* **2006**, *110*, 17370−17374.

(2) (a) Guillen, C.; Herrero, J. Structure, morphology and photoelectrochemical activity of $CuInSe_2$ thin films as determined by the characteristics of evaporated metallic precursors. *Sol. Energy Mater. Sol. Cells* **2002**, *73*, 141−149. (b) Cahen, D.; Gilet, J.-M.; Schmitz, C.; Chernyak, L.; Gartsman, K.; Jakubowicz, A. Room-Temperature, Electric Field-Induced Creation of Stable Devices in $CuInSe_2$ Crystals. *Science* **1992**, *258*, 271−274.

(3) (a) Bar, M.; Repins, I.; Contreras, M. A.; Weinhardt, L.; Noufi, R.; Heske, C. Chemical and electronic surface structure of 20%-efficient $Cu(In,Ga)Se_2$ thin film solar cell absorbers. *Appl. Phys. Lett.* **2009**, *95*, 052106−052106−3. (b) Chen, G. S.; Yang, J. C.; Chan, Y. C.; Yang, L. C.; Huang, W. Another route to fabricate single-phase chalcogenides by post-selenization of Cu−In−Ga precursors sputter deposited from a single ternary target. *Sol. Energy Mater. Sol. Cells* **2009**, *93*, 1351−1355. (c) Repins, I.; Contreras, M. A.; Egaas, B.; DeHart, C.; Scharf, J.; Perkins, C. L.; To, B.; Noufi, R. 19.9%-efficient $ZnO/CdS/CuInGaSe_2$ Solar Cell with 81.2% Fill Factor. *Prog. Photovoltaics Res. Appl.* **2008**, *16*, 235−239. (d) Caballero, R.; Guillen, C. $CuInSe_2$ Formation by selenization of sequentially evaporated metallic layers. *Sol. Energy Mater. Sol. Cells* **2005**, *86*, 1−10.

(4) (a) Wang, W.; Han, S.-Y.; Sung, S.-J.; Kim, D.-H.; Chang, C.-H. 8.01% $CuInGaSe_2$ solar cells fabricated by air-stable low-cost inks. *Phys. Chem. Chem. Phys.* **2012**, *14*, 11154−11159. (b) Wang, W.; Su, Y.-W.; Chang, C.-H. Inkjet printed chalcopyrite $CuIn_xGa_{1-x}Se_2$ thin film solar cells. *Sol. Energy. Mater. Sol. Cells* **2011**, *95*, 2616−2620. (c) Weil, B.; Conner, S. T.; Cui, Y. $CuInS_2$ Solar Cells by Air-Stable Ink Rolling. *J. Am. Chem. Soc.* **2010**, *132*, 6642−6643.

(5) (a) Todorov, T. K.; Gunawan, O.; Gokmen, T.; Mitzi, D. B. Solution-processed $Cu(In,Ga)(S,Se)_2$ absorber yielding a 15.2% efficient solar cell. *Prog. Photovoltaics Res. Appl.* **2012**, DOI: 10.1002/pip.1253. (b) Liu, W.; Mitzi, D. B.; Yuan, M.; Kellock, A. J.; Chey, S. J.; Gunawan, O. 12% Efficiency $CuIn(Se,S)_2$ Photovoltaic Device Prepared Using a Hydrazine Solution Process. *Chem. Mater.* **2010**, *22*, 1010−1014. (c) Mitzi, D. B.; Yuan, M.; Liu, W.; Kellock, A. J.; Chey, S. J.; Gignac, L.; Schrott, A. G. Hydrazine-based deposition route for device-quality CIGS films. *Thin Solid Films* **2009**, *517*, 2158−2162. (d) Mitzi, D. B. Solution Processing of Chalcogenide Semiconductors via Dimensional Reduction. *Adv. Mater.* **2009**, *21*, 3141−3158. (e) Mitzi, D. B.; Yuan, M.; Liu, W.; Kellock, A. J.; Chey, S. J.; Deline, V.; Schrott, A. G. A High-Efficiency Solution-Deposited Thin-Film Photovoltaic Device. *Adv. Mater.* **2008**, *20*, 3657−3662.

(6) Sotaniemi, E.; Hivonen, J.; Isomaki, H.; Takkunen, J.; Kaila, J. Hydrazine toxicity in the human. Report of a fatal case. *Ann. Clin. Res.* **1971**, *3*, 30−33.

(7) Panthani, M. G.; Akhavan, V.; Goodfellow, B.; Schmidtke, J. P.; Dunn, L.; Dodabalapur, A.; Barbara, P. F.; Korgel, B. A. Synthesis of $CuInS_2$, $CuInSe_2$, and $Cu(In_xGa_{1-x})Se_2$ (CIGS) Nanocrystal "Inks" for Printable Photovoltaics. *J. Am. Chem. Soc.* **2008**, *130*, 16770−16777.

(8) (a) Chang, S.-H.; Chiang, M.-Y.; Chiang, C.-C.; Yuan, F.-W.; Chen, C.-Y.; Chiu, B.-C.; Kao, T.-L.; Lai, C.-H.; Tuan, H.-Y. Facile colloidal synthesis of quinary $CuIn_{1-x}Ga_x(S_ySe_{1-y})_2$ (CIGSSe) nanocrystal inks with tunable band gaps for use in low-cost photovoltaics. *Energy Environ. Sci.* **2011**, *4*, 4929−4932. (b) Ahn, S. J.; Kim, K. H.; Yoon, K. H. Nanoparticle derived $Cu(In, Ga)Se_2$ absorber layer for thin film solar cells. *Colloids Surf. A* **2008**, *313−314*, 171−174. (c) Ahn, S. J.; Kim, C. W.; Yun, J. H.; Lee, J. C.; Yoon, K. H. Effects of heat treatments on the properties of $Cu(In,Ga)Se_2$ nanoparticles. *Sol. Energy Mater. Sol. Cells* **2007**, *91*, 1836−1841. (d) Li, B.; Xie, Y.; Huang, J.; Qian, Y. Synthesis by a Solvothermal Route and Characterization of $CuInSe_2$ Nanowhiskers and Nanoparticles. *Adv. Mater.* **1999**, *11*, 1456−1459.

(9) (a) Norako, M, E.; Brutchey, R. L. Synthesis of Metastable Wurtzite $CuInSe_2$ Nanocrystals. *Chem. Mater.* **2010**, *22*, 1613−1615. (b) Qiu, J.; Jin, Z.; Wu, W. B.; Xiao, L.-X. Characterization of $CuInS_2$ thin films prepared by ion layer gas reaction method. *Thin Solid Films* **2006**, *510*, 1−5.

(10) Guo, Q.; Ford, G. M.; Agrawal, R.; Hillhouse, H. W. Ink formulation and low-temperature incorporation of sodium to yield 12% efficient $Cu(In,Ga)(S,Se)_2$ solar cells from sulfide nanocrystal inks. *Prog. Photovoltaics Res. Appl.* **2012**, DOI: 10.1002/pip.2200.

(11) Yoon, S.; Yoon, T.; Lee, K.-S.; Yoon, S.; Ha, J. M.; Choe, S. Nanoparticle-based approach for the formation of CIS solar cells. *Sol. Energy. Mater. Sol. Cells* **2009**, *93*, 783−788.

(12) Bensebaa, F.; Durand, C.; Aouadou, A.; Scoles, L.; Du, X.; Wang, D.; Page, Y. L. A new green synthesis method of $CuInS_2$ and $CuInSe_2$ nanoparticles and their integration into thin films. *J. Nanopart. Res.* **2009**, *12*, 1897−1903.

(13) (a) Palchik, O.; Kerner, R.; Gedanken, A.; Weiss, A. M.; Slifkin, M. A.; Palchik, V. Microwave-assisted polyol method for the preparation of CdSe "nanoballs. *J. Mater. Chem.* **2001**, *11*, 874−878. (b) Palchik, O.; Kerner, R.; Zhu, J.; Gedanken, A. Preparation of $Cu_{2-x}Te$ and HgTe by Using Microwave Heating. *J. Solid State Chem.* **2000**, *154*, 530−534. (c) Zhu, J.; Palchik, O.; Chen, S.; Gedanken, A. Microwave Assisted Preparation of CdSe, PbSe, and $Cu_{2-x}Se$ Nanoparticles. *J. Phys. Chem. B* **2000**, *104*, 7344−7347. (d) Wu, C.-C.; Shiau, C.-Y.; Ayele, D. W.; Su, W.-N.; Cheng, M.-Y.; Chiu, C.-Y.; Hwang, B.-J. Rapid Microwave-Enhanced Solvothermal Process for Synthesis of $CuInSe_2$ Particles and Its Morphologic Manipulation. *Chem. Mater.* **2010**, *22*, 4185−4190. (e) Sun, C.; Gardner, J. S.; Long, G.; Bajracharya, C.; Thurber, A.; Punnoose, A.; Rodriguez, R. G.; Pak, J. J. Controlled Stoichiometry for Quaternary $CuIn_xGa_{1-x}S_2$ Chalcopyrite Nanoparticles from Single-Source Precursors via Microwave Irradiation. *Chem. Mater.* **2010**, *22*, 2699−2701. (f) Grisaru, H.; Palchik, O.; Gedanken, A.; Palchik, V.; Slifkin, M. A.; Weiss, A. M. Microwave-Assisted Polyol Synthesis of $CuInTe_2$ and $CuInSe_2$ Nanoparticles. *Inorg. Chem.* **2003**, *42*, 7148−7155.

(14) Jeong, S.; Lee, B.-S.; Ahn, S. J.; Yoon, K. H.; Seo, Y.-H.; Choi, Y.; Ryu, B.-H. An 8.2% efficient solution-processed $CuInSe_2$ solar cell based on multiphase $CuInSe_2$ nanoparticles. *Energy Environ. Sci.* **2012**, *5*, 7539−7542.

(15) Whittaker, A. G.; Mingos, D. M. P. Arcing and other microwave characteristics of metal powders in liquid systems. *J. Chem. Soc., Dalton Trans.* **2000**, 1521−1526.

(16) Seo, Y.-H.; Prasetyanto, E. A.; Jiang, N.; Oh, S.-M.; Park, S.-E. Catalytic dehydration of methanol over synthetic zeolite W. *Microporous Mesoporous Mater.* **2010**, *128*, 108−114.

(17) (a) Chow, G. M.; Kurihara, L. K.; Ma, D.; Feng, C. R.; Schoen, P. E.; Martinez-Miranda, L. J. Alternative approach to electroless Cu metallization of AlN by a nonaqueous polyol process. *Appl. Phys. Lett.* **1997**, *70*, 2315−2317. (b) Hegde, M. S.; Larcher, D.; Dupont, L.; Beaudoin, B.; Tekaia-Elhsissen, K.; Tarascon, J.-M. Synthesis and chemical reactivity of polyol prepared monodisperse nickel powders. *Solid State Ionics* **1997**, *93*, 33−50. (c) Fievet, F.; Lagier, J. P.; Figlarz,

M. Preparing monodisperse metal powers in micrometer and submicrometer sizes by the polyol process. *MRS Bull.* **1989**, *14*, 29–34.

(18) (a) Ksapabutr, B.; Gulari, E.; Wongkasemjit, S. One-pot synthesis and characterization of novel sodium tris(glycozirconate) and cerium glycolate precursors and their pyrolysis. *Mater. Chem. Phys.* **2004**, *83*, 34–42. (b) Zhao, J.; Fan, W.; Wu, D.; Sun, Y. Synthesis of highly stabilized zirconia sols from zirconium n-propoxide-diglycol system. *J. Non-Cryst. Solids.* **2000**, *261*, 15–20. (c) Jansen, M.; Guenther, E. Oxide Gels and Ceramics Prepared by a Nonhydrolytic Sol-Gel Process. *Chem. Mater.* **1995**, *7*, 2110–2114. (d) Stefanescu, M.; Stoia, M.; Stefanescu, O. Thermal and FT-IR study of the hybrid ethylene-glycol–silica matrix. *J. Sol-Gel Sci. Technol.* **2007**, *41*, 71–78.

(19) (a) Parretta, A.; Addonizio, M. L.; Loreti, S.; Quercia, L.; Jayaraj, M. K. An investigation on the growth of thin chalcopyrite $CuInSe_2$ films by selenization of Cu-In alloys in a box. *J. Cryst. Growth* **1998**, *183*, 196–204. (b) Jackson, S. C.; Baron, B. N.; Rocheleau, R. E.; Russel, T. W. F. A chemical reaction model for physical vapor deposition of compound semiconductor films. *AIChE J.* **1987**, *33*, 711–721.

(20) Kwon, O.-J.; Yoon, D. N. Closure of Isolated Pores in Liquid Phase Sintering of W-Ni. *Int. J. Powder Metall. Powder Technol.* **1981**, *17*, 127–134.

(21) (a) Kim, K.; Eo, Y.-J.; Cho, A.; Gwak, J.; Yun, J. H.; Shin, K.; Ahn, S. K.; Park, S. H.; Yoon, K.; Ahn, S. J. Role of chelate complexes in densification of $CuInSe_2$ (CIS) thin film prepared from amorphous Cu–In–Se nanoparticle precursors. *J. Mater. Chem.* **2012**, *22*, 8444–8448. (b) Ahn, S. J.; Kim, C. W.; Yun, J. H.; Gwak, J.; Jeong, S.; Ryu, B.-H.; Yoon, K. H. $CuInSe_2$ (CIS) Thin Film Solar Cells by Direct Coating and Selenization of Solution Precursors. *J. Phys. Chem. C* **2010**, *114*, 8108–8113. (c) Kaelin, M.; Rudmann, D.; Kurdesau, F.; Zogg, H.; Meyer, T.; Tiwari, A. N. Low-cost CIGS solar cells by paste coating and selenization. *Thin Solid Films* **2005**, *480–481*, 486–490.